Electron Attachment in Ice−HCl Clusters: An ab Initio Study

Xifeng Li and Léon Sanche

Département de Médecine Nucléaire et de Radiobiologie, Faculté de Médecine, Université de Sherbrooke, Québec, Canada

Arvi Rauk and David Armstrong*

Department of Chemistry, University of Calgary, Alberta, Canada

Received: December 6, 2004; In Final Form: March 4, 2005

Experimental work has shown that small amounts of HCl strongly enhance electron capture in ice films. The purpose of the present study was to investigate the effect of adsorbed HCl on the interaction of electrons with small clusters of water. Studies were made with clusters of 6 and 12 water molecules with various geometries both with and without one HCl attached. A number of distinct HCl coordination motifs were examined. All of the neutral structures with HCl exhibited zero thresholds for electron attachment and formed dipole bound anionic states (DBS). The relaxation processes for these "initial DBS" depended on the number of H_2O (n) and on the number and type of H-bonds to the HCl (x). The initial DBS of systems with only O−H···Cl H-binding underwent dissociative electron attachment (DEA), forming H atoms. Relaxation for systems with ClH···OH_2 bonds was more complex. For the two layer $n = 12$ systems with $x = 2$ or 3 the HCl proton moved to the nearest oxygen to form H_3O^+. Then rearrangement of the proton network occurred, and the Cl^- became solvated by three HO−H···Cl^- bonds. The presence of Cl^- and H_3O^+ increases the dipole moment and the electron binding energy (EBE) of the network. Further stabilization is achieved by decay into deeper DBS electron traps and/or by reaction of the excess electron with H_3O^+ to form H• atoms. The $HCl(H_2O)_6$ clusters with a single Cl−H···OH_2 bond behaved differently. They increased their stability by becoming more linear. This raised the dipole moment and the EBE therefore increased, reducing the total energy. None of these species showed any signs of increasing the number of H-bonds to Cl. The implication of these observations for the interpretation of the results of the experiments with 0.2 monolayer of HCl on 5 monolayer of H_2O at 20 K, and on the possible role of cosmic ray-induced ionization in polar stratospheric clouds in ozone depletion is discussed.

Introduction

During the past few decades the structures and properties of ice clusters containing HCl and other acids have been studied extensively.[1−7] There are a number of reasons for this. First, heterogeneous reactions on polar stratospheric ice clouds (PSCs), including reactions of HCl, are now known to be key processes in the depletion of ozone in polar regions.[1,8,9] Studies of reactions on ice particles and films are therefore of considerable practical importance. Second, as the water:HCl ratio in clusters rises, the structure of HCl exhibits a transition from a hydrogen bonded neutral ClH···OH_2 toward a Cl^-···HOH_2^+ ion pair. Examination of the sequence of changes allows one to gain an understanding of the process of acid ionization in solution.[4,6] A third feature, which has come to light more recently, is the fact that the peak energy for electron attachment to HCl is reduced to zero energy and the cross section is increased severalfold when it is adsorbed on an ice film.[10] This has been attributed to a large enhancement in the cross section for electron attachment near 0 eV electron energy. Like the acid ionization this is undoubtedly due to the lowering of potential barriers by the solvating effect of the H_2O molecules, which stabilizes polar and ionic species. However, the details of the process are yet to be understood.

The purpose of this study was to use ab initio methods to investigate the interaction of low energy electrons with ice particles in the presence and absence of adsorbed HCl. An important objective was to use $HCl(H_2O)_n$ structures, which would be similar to those that obtained in the experimental study of the electron capture.[10] Here the ice consisted of 5 monolayers (ML) of H_2O deposited on 10 ML of Kr at 20 K. A 0.2 ML of HCl was then deposited on the ice at the same temperature. H_2O molecules are not expected to be mobile at this temperature and relaxation would be largely confined to nearest neighbors.[11] HCl would therefore be located primarily on the ice surface. The ice was considered to be amorphous and probably porous, because of the temperature of deposition.[11,12] There are therefore likely to be a variety of different types of environment for the HCl. In terms of H-bonding to H_2O, HCl is a poor H acceptor, but a good donor. Thus, the primary interaction is expected to be Cl−H···OH_2, with secondary O−H···Cl bonds to the Cl in sites where dangling hydrogens are suitably located.[2,4,6,7] The primary site leads to singly coordinated HCl, while the addition of O−H···Cl bonds may lead to doubly or triply coordinated HCl, depending on the number of O−H···Cl bonds. Triply coordinated HCl in clusters with four or more H_2O is generally ionized. Ionization does not occur with fewer waters or lower coordination, but the H−Cl bond is increasingly polarized and extended as stabilization by H_2O increases.[4,6,7] HCl singly or doubly H-bonded purely by HO−H···Cl bonds is expected to be rare.

* Corresponding author. E-mail: armstron@ucalgary.ca.

10.1021/jp044459h CCC: $30.25
Published on Web 04/22/2005

Models of HCl-ice clusters were made by adding HCl to a variety of H-acceptor sites on previously prepared $(H_2O)_6$ and $(H_2O)_{12}$ structures. The $(H_2O)_{12}$ structure was designed to mimic the upper layers of the multilayer ice film and consisted of two layers of $(H_2O)_6$ H-bonded together. The top layer was optimized while retaining the hexagonal structure in the lower layer. The geometry of this optimized top layer was also used as a model of an amorphous $(H_2O)_6$ cluster. HCl was bonded to several different O atom sites of the $(H_2O)_6$ and $(H_2O)_{12}$ structures and the coordination number was varied. Finally, although it is expected to be rare, a site with HCl held by O−H···Cl bonds and no Cl−H···OH_2 bond was examined.

The water dimer and H_2O···HCl are both known to attach electrons to form dipole bound anion states (DBS).[13−15] DBS of larger water clusters have also been observed experimentally and studied extensively by ab initio methods.[16−19] Thus, DBS formation may be expected as the initial step in electron attachment in many of these models, and indeed this was found to be the case. The changes in energy, which occurred on the vertical attachment of electrons, were determined for every structure, so that threshold energies for attachment with and without HCl could be compared. Also subsequent reactions of electrons in $HCl(H_2O)_n$ traps were followed by carrying out optimizations of the species formed by vertical attachment. These reactions were in themselves intrinsically interesting. For convenience, 1, 2, and 3-coordinated structures are designated as (HCl(*x*)/*n*), where *x* indicates the total number of H-bonds, the first one being a Cl−H···OH_2, and *n* is the number of H_2O. For example (HCl(2)/12) means that HCl is attached to $12H_2O$ with one Cl−H···OH_2 bond and one O−H···Cl bond. Pure HO−H···Cl bonding is specified explicitly.

Computational Methods

The ab initio calculations were performed with the Gaussian 98 and 03 molecular orbital packages.[20,21] Due to the size of the systems, the B3LYP functional was employed in most cases. The geometries of neutral $(H_2O)_6$ and $(H_2O)_{12}$ ice clusters with and without HCl were obtained at the B3LYP/6-31G(d) level. Electronic energies were obtained from B3LYP/aug-cc-pVDZ level calculations on the B3LYP/6-31G(d) geometries. Binding energies (BEs) of HCl on the Born Oppenheimer surface (BOs) were obtained from the differences in electronic energies: $\Delta E = E(\mathrm{HCl}) + E(\mathrm{H_2O})_n - E(\mathrm{HCl(H_2O)}_n)$, at the B3LYP/aug-cc-pVDZ level. Basis set superposition errors at this level are not expected to be significant[22] and were not made.

The B3LYP method has generally been found to perform satisfactorily for calculating structures of ice clusters and their DBS.[4,17] It also performs reasonably well in computing the energies of closed shell clustered ions.[23] However, it tends to overestimate electron binding in DBS, often by a few tenths of an eV, and electron binding energies in DBS should be obtained at the CCSD(T) level.[16,24] Also normal basis sets must be augmented by diffuse functions in order to accommodate the large orbitals occupied by the excess electron.[13−16] Typically these consist of sets of s-, p-, and d-type Gaussian functions with decreasing exponents (0.005625, 0.001125, 0.000225, and 0.000045), added in this order until the binding energy is converged. In the present work with the anions of some of the $(H_2O)_6$ systems, CCSD(T) level calculations with 6-31G(d) or 6-31+G(d) basis sets and up to four additional sets of diffuse functions were carried out. These represented the maximum basis sets possible with our resources. The larger $(H_2O)_{12}$ systems could not be treated in this way. However, for these, the dipole moments were generally well above the critical value for DBS formation, and the B3LYP calculated binding energies are so large (∼0.4 eV) that DBS formation was not in doubt. It was also found (see below) that aug-cc-pVDZ basis sets were able to accommodate the electron without additional diffuse functions. Therefore, for the comparison of larger structures, both with and without HCl, electron binding energies were routinely determined from B3LYP/aug-cc-pVDZ single-point calculations on neutral and anion geometries. Unless stated otherwise, these are the ones referred to in the text.

Binding energies of the electron on the BOs of neutral and anion geometries are referred to here as EBEs. For the specific case where the anion geometry is the same as the neutral (i.e., the attachment is vertical), the abbreviation VBE is used. The fact that frequencies (and ZPEs) for DBS anions are generally lower than those of the neutrals[25,26] means that in principle EBEs and VBEs are lower limits for EAs and vertical attachment energies, respectively. It should be noted that EBEs and VBEs were always calculated from electronic energies with the same basis sets on the neutral and anion. Contour plots of the singly occupied molecular orbitals (SOMOs) of DBSs were obtained from B3LYP/aug-cc-pVDZ level calculations using gOpenMol version 2.32.[27] Dipole moments of neutrals were also obtained at this level.

As a means of determining what relaxation pathways would be available to the initially formed negative ion species, their structures were optimized. In the experiments, the exposed H_2O in upper layers of ice, where HCl would attach, are subject to structural limitations imposed by bonding to lower H_2O layers. To mimic this effect, many of the optimizations were carried out with geometric restrictions to parts of the structures. Optimizations of anions of $HCl(H_2O)_6$ clusters were first performed at the B3LYP/6-31+G(d) level with the ice base frozen. Subsequently, they were re-optimized at the B3LYP/aug-cc-pVDZ with no geometry restrictions. Restrictions applied for other systems are described in the Results section. Optimization of $HCl(H_2O)_{12}$ anions at B3LYP/aug-cc-pVDZ level or B3LYP/6-31+G(d) proved to be impractical. They were optimized at the B3LYP/6-31G(d) level. These small basis sets tend to force the electron into a valence level. However, further optimizations and scans of energy changes during bond dissociation were carried out with diffuse functions added to accommodate DBS electrons.

Finally, the open structure H_2O···HO−H···ClH was used as a model of a system with HCl held only by O−H···Cl bonds. This system was studied at the MP2/aug-cc-pVDZ level.

Results

This section starts with a description of the four ice models. Then results for HCl in triply, doubly, and singly coordinating sites are presented. In each case, we first examine the VBE and then the relaxation processes which may take place after electron attachment. In general, all types of HCl coordination exhibit zero-energy thresholds for electron attachment. However, the subsequent relaxation processes depend on the type of coordination and the size of the cluster. Comparisons of the various systems and conclusions are given in the Discussion.

1. Structures for the Simulation of the 20 K Ice Film. It was evident that different sites would be required in order to provide examples of 1, 2, and 3 coordination of HCl to amorphous ice. Also the number of H_2O molecules had to be large enough to simulate the effect of multilayers and provide a realistic level of stabilization of ionic and polar species. A variety of minimum energy structures of H_2O clusters obtained by ab initio methods have been reported. For example, see ref

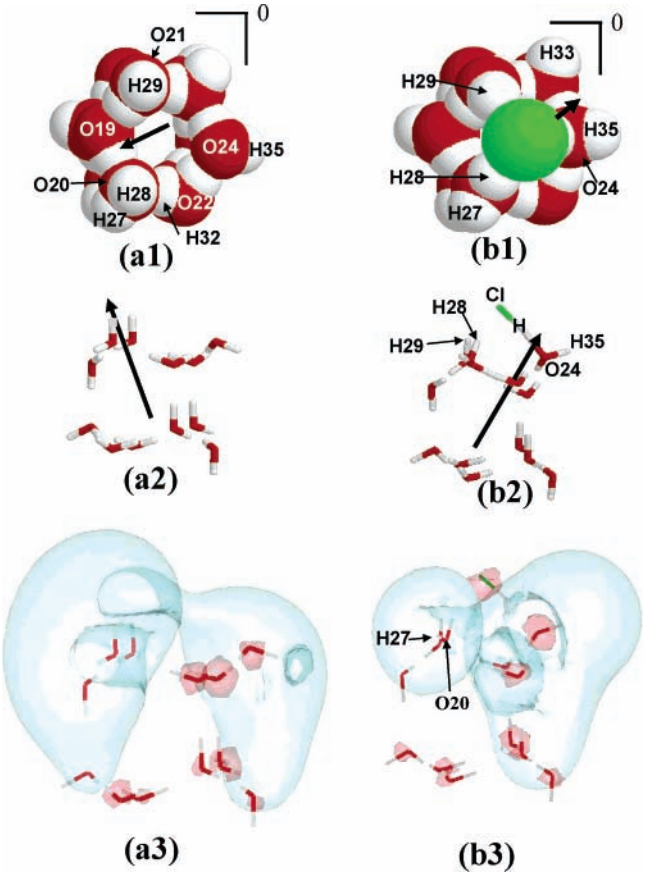

Figure 1. Structures and SOMO contours for two layered hexagonal $(H_2O)_{12}$: (a1), (a2), (a3); and triply coordinated $HCl(H_2O)_{12}$ with hexagonal ice base: (b1), (b2), (b3). (a1) and (a2) are top and side views of the neutral $(H_2O)_{12}$ structure, and (a3) shows the contour of the SOMO of the DBS of this geometry containing 0.5 electron. (b1), (b2) and (b3) are corresponding views of triply coordinated $HCl(H_2O)_{12}$. Heavy arrows indicate directions of dipole moment vector for the neutrals, and atoms referred to in the text are numbered.

28. However, in this instance it was decided to derive structures which had an initial relationship to hexagonal ice. The method is described below. The choice of HCl binding sites is explained later.

(a) Hexagonal $(H_2O)_{12}$ Cluster. A two layer $(H_2O)_{12}$ cluster with hexagonal ice structure, based on the P-ice model of ref 29, was used as a starting point. The O atoms were in a tetrahedral geometry and all r(O−O) were fixed at the experimental value of 2.74 Å.[30,31] The equilibrium positions of the hydrogens were obtained by optimizing at the B3LYP/6-31G-(d) level with bonds of the same type treated as single variables, i.e., all r(O−H) for free H were the same and all r(O−H) for H-bonding H the same. The dimensions obtained were r(O−H) for free H = 0.972 Å; r(O−H) for H-bonding = 0.985 Å. The geometry is depicted in Figure 1, parts a1 and a2. Part a1 is a space filling model looking down the hexagonal channel, whereas part a2 is a stick model showing a side view. In a large ice structure, the dangling Hs in each $(H_2O)_6$ layer would be H-bonded to other waters. Their presence here means that the surface energy is not minimized.

The dipole moment of the $(H_2O)_{12}$ hexagonal ice cluster was 6.0 D (see dipole vector arrows in Figure 1, parts a1 and a2), and well above the critical value of 2.2 D for the binding of an electron in a dipole bound anion state.[32,33] At the B3LYP/6-31G(d)//B3LYP/6-31G(d) level, the VBE was negative. The B3LYP/aug-cc-pVDZ//B3LYP/6-31G(d) value was 0.491 eV. With the addition of one spd, two spd, and two spd + one sp diffuse functions to O20, which is near the positive end of the dipole (Figure 1a1), the VBEs were 0.550, 0.553, and 0.553 eV, respectively. As stated in the previous section, EBEs and VBEs were routinely evaluated at the B3LYP/aug-cc-pVDZ level without additional diffuse functions. Using these results slightly reduces the B3LYP error at the converged level.[34] The SOMO of the DBS of the above structure is shown in Figure 1a3. Maximum density is clustered around the dangling H atoms nearest the positive end of the dipole. However, there is substantial density on other dangling Hs and the shape is noticeably less regular than the SOMOs of octamers and other large water structures, where the dipoles were more maximally aligned and/or dangling Hs tended to be clustered together.[19,35] Thus, local dipoles must also play a role.

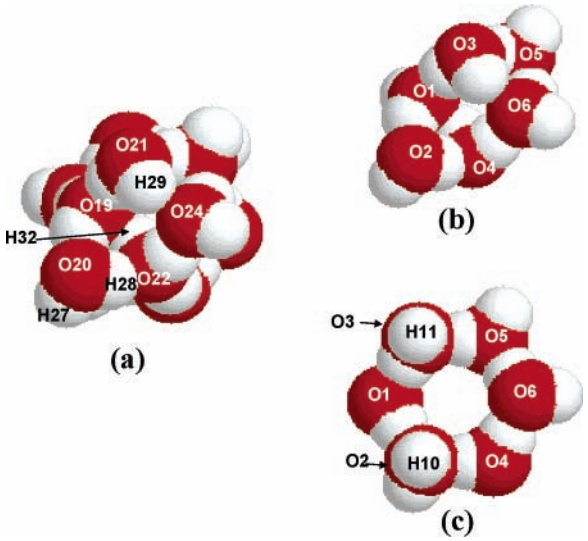

Figure 2. Top views of structures of: (a) two layered $(H_2O)_{12}$ with hexagonal base and optimized upper layer; (b) structure (upper layer of (a)) and numbering scheme used for the amorphous $(H_2O)_6$ model. (c) structure and numbering scheme used for the hexagonal $(H_2O)_6$ model.

(b) $(H_2O)_{12}$ Cluster: Upper Layer Optimized. Although the internal structure of ice particles may be hexagonal, the surface layers are less ordered.[11] Dangling Hs are less frequent and the surface energy is reduced. The hexagonal $(H_2O)_{12}$ cluster was therefore re-optimized at the B3LYP/6-31G(d) level with no restrictions on the bonding parameters of the upper $(H_2O)_6$ layer, except that it was H-bonded to the lower layer. The latter was again kept in a hexagonal (Os tetrahedral) geometry and all r(O−H) for free H and r(O−H) for H-bonding H were, respectively, the same. The O−H···O distances between O atoms in the top and bottom layers now varied between 2.71 and 2.78 Å. As shown by the top view of the structure in Figure 2a, the dangling hydrogens H29 and H28 H-bonded respectively to O24 and O22 (Compare Figure 1a1). At the same time H32 was reoriented to H-bond to O19. The B3LYP/6-31G(d)//B3LYP/6-31G(d) energy was lowered by 64 kJ/mol. The dipole moment was reduced from 6.0 to 3.8 D and the B3LYP/aug-cc-pvdz//B3LYP/6-31G(d) VBE fell from 0.49 to 0.31 eV.

(c) $(H_2O)_6$ Clusters. Figure 2b shows the $(H_2O)_6$ framework of the upper layer of the above $(H_2O)_{12}$. The dipole moment of this cluster is now quite low, 0.58 D, and the VBE is negative (−0.04 eV). These values and the presence of the cross ring O−H···O bonds are more typical of what may be expected for H_2O clusters in an amorphous ice network where dangling Hs are minimized. The geometry and numbering system used for the $(H_2O)_6$ cluster is shown in the figure (Rather than using the original numbers from Figure 2a, the atoms are renumbered 1

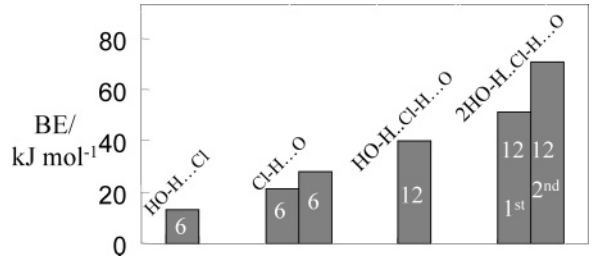

Figure 3. Effect of coordination type on Born Oppenheimer binding energies (in kJ mol^{-1}) of HCl to $(H_2O)_n$ clusters. The value of n is shown on each bar. The data for Cl−H···O give the range observed for single coordination to $n = 6$ amorphous systems, and for $_2$HO−H···Cl−H···O the results for the initial (first) and rearranged neutral (second) (see text) are shown.

to 18 for simplicity). We refer to this as the amorphous $(H_2O)_6$. Studies made with HCl H-bonded to oxygens 2, 3, 4, and 5 are described below. Studies were also made with HCl at several positions on the $(H_2O)_6$ upper layer of the $(H_2O)_{12}$ cluster with the hexagonal ice structure (see Figure 2c), which was similarly renumbered. Due to the residual dangling Hs, this hexagonal $(H_2O)_6$ has a much larger dipole moment (4.4 D) and a VBE of 0.22 V. On the other hand its energy is 39 kJ mol^{-1} above that of the amorphous $(H_2O)_6$. Dipole moments, relative energies and electron binding energies for the $(H_2O)_6$ and $(H_2O)_{12}$ neutral clusters have been summarized in Table S1.

2. Triply Coordinated $HCl(H_2O)_{12}$ Systems: (HCl(3)/12). The O24 site in the $(H_2O)_{12}$ hexagonal cluster (Figure 1a1) provides a base for a primary Cl−H···O H bond, and the nearby H28 and H29 make it a good site for 3 coordination binding. HCl was placed in this position. The geometry was then optimized with all of the atoms in the top layer free, but the Os in the bottom held in tetrahedral geometry (i.e., as described above for the $(H_2O)_{12}$ Cluster: Upper Layer Optimized). The resulting structure is shown in Figure 1, parts b1 and b2. The BE of HCl for this structure was 55 kJ mol^{-1}. This and other BEs for (HCl(*x*)/*n*) neutrals are plotted in Figure 3.

The Cl−H distance in the neutral (HCl(3)/12) structure in Figure 1 is increased from 1.285 Å in free HCl to 1.372 Å and the H···O24 distance is 1.553 Å, indicating polarization of the Cl−H bond and motion of the proton toward the oxygen. This is similar to observations made previously.[6] Additivity of dipoles in the Cl−H−O24−H35 fragment will make a large contribution to the overall dipole moment. Because of this and the capping of H28 and H29 by the electronegative Cl, the direction of the dipole vector is reoriented from that of the hexagonal $(H_2O)_{12}$ cluster (compare parts a1 and 2 with parts b1 and 2 in Figure 1). The magnitude of the dipole moment (5.5 D) is relatively unchanged and again large enough to form a DBS. The DBS with the geometry of the neutral, which as in all cases in this work is referred to as the "primary DBS" (DBS′), has an VBE of 0.45 eV at the B3LYP/aug-cc-pVDZ//B3LYP/6-31G(d) level. In this case the adequacy of the smaller 6-31G-(d) basis sets to accommodate the excess electron in the presence of diffuse functions was also tested. Addition of one set of spd functions on the Cl caused the VBE to rise from −1.71 to +0.354 eV. The second spd set raised it to 0.366 eV, and addition of a further sp set gave 0.368 eV. The last is not yet near the value with the aug-cc-pVDZ basis set, but clearly most of the effect of the diffuse functions is accommodated with the first spd. This finding was important because of the necessity to use the 6-31G(d) + 1 spd basis set combinations in optimizations and bond dissociation scans, which are described later. The SOMO of (HCl(3)/12) DBS′ at the B3LYP/aug-cc-pVDZ level is shown in Figure 1b3. There is a small lobe on H27, but the density is now greatest near O24 and H35 (see parts b1 and b2 for atom positions) and the aug-cc-pVDZ Mulliken spin and charge distributions (not given here) reflect that.

As a means of exploring what subsequent reactions might occur and examining the relative stability of alternative structures, this anion was optimized with all of the atoms in the top layer free, but the Os in the bottom again held in tetrahedral geometry to simulate the retarding effect of H-bonding to lower layers in multilayer ice films at 20 K. Optimization was carried out at the B3LYP/6-31G(d) level. In the first phase the Cl−H distance increases, the negative charge on Cl rises and the proton moves to O24. At $r_{(Cl-H)} = 2$ Å the Cl charge is −0.7, the O24 site becomes a hydronium ion and the spin is largely on H35 and H33 (see positions in Figure 1, parts b1 and b2). Subsequently the O24−H35 distance increases and this proton eventually takes the electron, becoming a free H atom, i.e., the system underwent reaction 1

$$HCl(H_2O)_n^{\bullet -} \rightarrow H^{\bullet} + Cl^{-}(H_2O)_n \qquad (1)$$

An optimized structure of the $H^{\bullet}\cdots Cl^{-}(H_2O)_{12}$ complex was obtained with an O24−H35 distance of 2.171 Å. (The structure of this is available in Table S2, whereas Table S3 contains the structure of the $Cl^{-}(H_2O)_{12}$ without the H atom). The energy profile as a function of the O24−H35 distance was then investigated at B3LYP/6-31G(d) level with one set of spd diffuse functions on O24 by optimizing other parameters in the top layer at fixed O24−H35 separations. aug-cc-pVDZ level energies of lowest energy structures along the path were calculated and have been plotted in Figure 4a relative to that of the initial neutral. These results indicate a minimum near 1 Å. Starting at that geometry and optimizing at the B3LYP/6-31G(d) level with one set of spd diffuse functions on O24 showed this to be much deeper and at $r_{(O24-H35)} = 0.975$ Å, only slightly longer than in the neutral (0.971 Å). This optimized DBS structure is shown in Figure 4b. The HCl is fully ionized, and the protons in the upper layer have undergone considerable rearrangement with O21 becoming a hydronium ion site (see arrow in Figure 4b). Figure 4c shows that the SOMO is now more concentrated on the O24 side of the cluster, the lobe on H27 in the (HCl(3)/12) DBS′ having been reduced (Figure 1b3). Removal of the electron and optimization of the resulting neutral gave a slightly different structure shown in Figure 4d. The HCl is still completely ionized, but the hydronium site has migrated to O19 (see arrows). The BE of HCl in this second neutral was 76 kJ mol^{-1}.

Based on the small basis sets used here one cannot claim that the species and stabilization pathways described above are unique. However, the present procedures demonstrate that very significant reactions can occur in a multilayer system. Figure 4a shows the B3LYP/aug-cc-pVDZ energies on the respective B3LYP/6-31G(d) geometries relative to the level of **1**, the original neutral, of: **2**, the initial DBS ((HCl(3)/12) DBS′); **3**, the optimized DBS; **4**, the second neutral; **5**, the $H^{\bullet}$ + $Cl^{-}\cdots(H_2O)_{12}$ dissociation products. The second neutral lies 0.48 eV below the initial one and slightly below the DBS′. The barrier to reach this from **1** on the neutral surface was not explored, but it is probably significant because the proton rearrangements are extensive. When formed, **2** contains the excess energy of electron binding (0.45 eV) and in principle could undergo a number of transformations: passage over the barrier to **5**; rearrangement to **4** and loss of the electron; or energy dissipation and stabilization to **3**. Given the large number of vibrational modes in which the excess energy may be distributed, the last process seems the most likely.

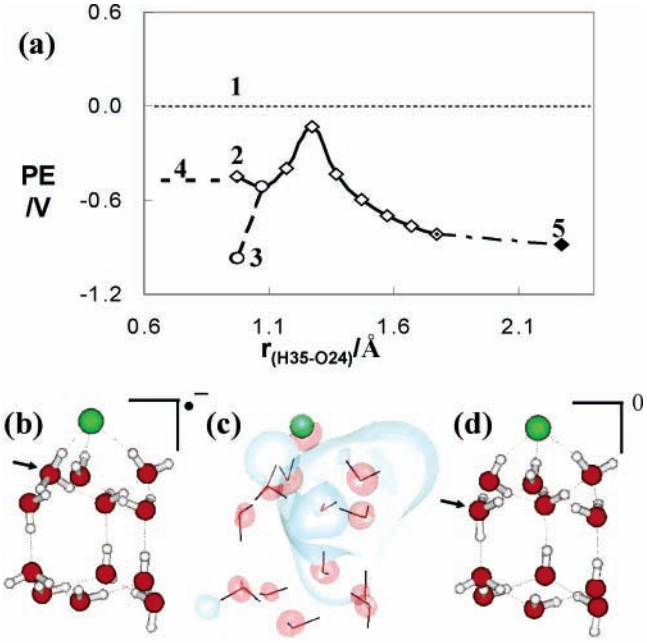

Figure 4. Energy changes and secondary structures observed in the stabilization of (HCl(3)/12) DBS′: (a) Energy as a function of $r_{(H35-O24)}$: energies of specific structures are indicated by numbers and are relative to the energy of the initial neutral, 1; 2 is the level of the DBS′ on the neutral geometry and 5 that of $H^{\bullet} + Cl^{-}\cdot(H_2O)_{12}$. (b) Optimized structure of the DBS, 3 (The $r_{(H35-24)}$ distance in this is 0.970 Å). (c) contour of the DBS SOMO containing 0.5 electron. (d) Structure of 4, the neutral derived on electron detachment from (b). The arrows on (b) and (d) indicate H_3O^+.

3. Doubly Coordinated $HCl(H_2O)_{12}$ Systems: (HCl(2)/12). The O20 site in the $(H_2O)_{12}$ Cluster: Upper Layer Optimized (Figure 2a) was used as a base for a primary Cl−H···O H-bond, and the nearby H29 then provided a O−H···Cl coordination. The geometry was optimized as in the (HCl(3)/12) case, keeping the Os in the bottom in tetrahedral geometry. The resulting neutral structure is shown in Figure 5, parts a1 and a2 (note that the structure in Figure 5a1 is rotated 120° clockwise from that in Figure 2a). Notably there was no tendency to form a third coordination. However, the O20 water moves out of the upper layer to better coordinate the Cl (Figure 5a2). The proton in the primary Cl···H···O H-bond does not move as close to the O as in (HCl(3)/12). The Cl···H and H···O distances here are 1.354 and 1.611 Å, respectively, as opposed to 1.372 and 1.553 Å in the former case. The BE of HCl for this structure was 43 kJ mol^{-1}, significantly smaller than for (HCl(3)/12), Figure 3. The overall dipole moment of the structure in Figure 5a2 is 1.2 D and below the critical value of 2.2 D for DBS formation.

Despite the low dipole moment, the anion with the geometry of the neutral in Figure 5a2 has a positive VBE of 0.34 eV. The SOMO (not shown) was diffuse and spread over the dangling Hs, mostly: Hs 9, 16, 17, 27, and 33 (see atom numbers in Figure 5, parts a1 and a2). Thus, it appears that this (HCl(2)/12) DBS′ state exists due to local dipoles. B3LYP/6-31G(d) level optimization with the top layer free and the Os in the bottom tetrahedral gave rise to significant changes. Quite early the upper water layer rearranges and the proton in the Cl−H···O bond moves to O20 to form H_3O^+. This interacts with O22, resulting in the formation of a $H_2O-H^+-OH_2$ Zündel ion involving O20 and O22. The upper layer then splits into two, three H_2Os binding the Cl^- and the second three holding the $Cl^-\cdots(H_2O)_3$ cluster to the lower six-member layer. The Zündel ion then breaks up and the proton moves to O23 forming

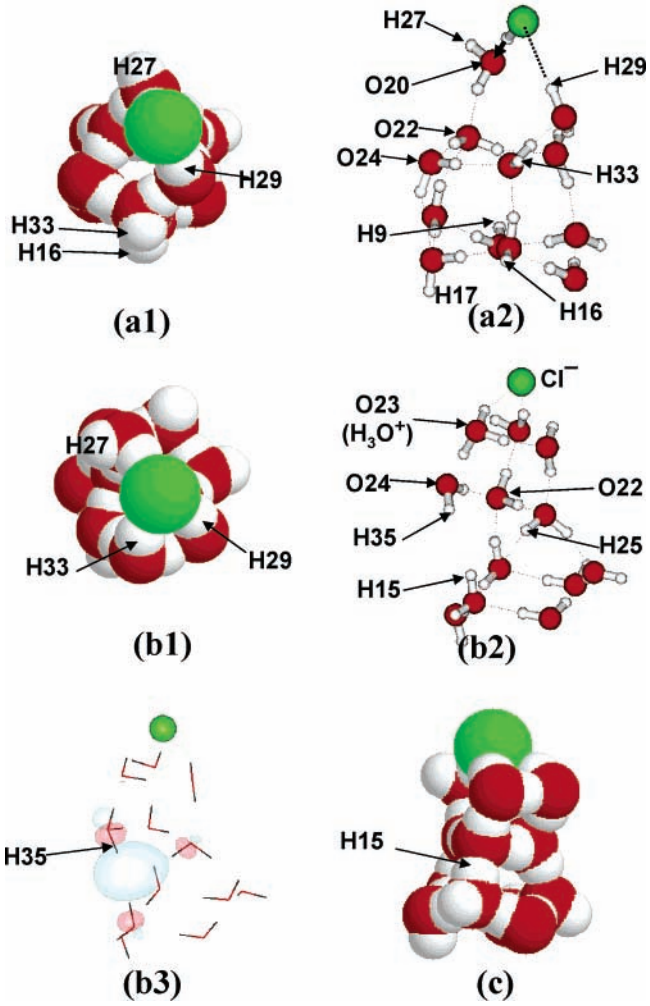

Figure 5. Structures observed for (HCl(2)/12). (a1) and (a2) are top and side views of the initial neutral; (b1) and (b2) top and side views and (b3) contour of the DBS SOMO containing 0.5 electron. (c) is the structure of the $Cl^-(H_2O)_{12}$ formed on loss of H 35. Atoms referred to in the text and H_3O^+ are labeled.

H_3O^+. At the same time H15, H25, and H35 point inward to form a compact electron trap. This very interesting B3LYP/6-31G(d) structure was optimized with a set of 2sp functions on H35. With minimal changes, it gave the stable structure in Figure 5, parts b1 and b2, which show the features described above. The coordinates are given in Table S4. The SOMO, Figure 5b3, is best described as the in-phase combination of the σ^* orbitals of the three OH bonds. The distribution of the electron is very tight and the B3LYP EBE has increased to 0.473 eV.

Continued optimization of the above intermediate without the 2sp functions caused H35, which in the Mulliken analysis contained 50% of the spin, to dissociate in reaction 1.

Optimization of the $Cl^-\cdots(H_2O)_{12}$ fragment gave the structure in Figure 5(c). As indicated in Figure 5, parts b2 and c, the loss of H35 allows H15 to hydrogen bond to O24 and close up the structure. The energy profile for H35 dissociation was not investigated as in Figure 4a for (HCl(3)/12). However, Figure 6 shows the B3LYP/aug-cc-pVDZ energies relative to neutral (HCl(2)/12) of the DBS′, the above intermediate as DBS and $H^{\bullet} + Cl^-\cdots(H_2O)_{12}$. Again the pathways seen are not necessarily unique. Especially interesting in this case is the split of the upper $(H_2O)_6$ into two layers. The structure of the $Cl^-\cdots(H_2O)_{12}$ solvated in this way is given in Table S5. Its energy is only 6 kJ mol^{-1} above the $Cl^-\cdots(H_2O)_{12}$ cluster obtained for dissocia-

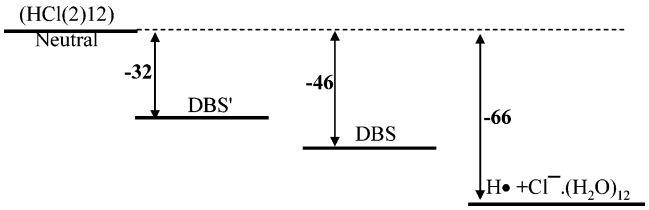

Figure 6. Energies in kJ mol^{-1} of the DBS and the H$^{\bullet}$ +Cl^{-}•$(H_2O)_{12}$ dissociation products for (HCl(2)/12) species relative to the neutral.

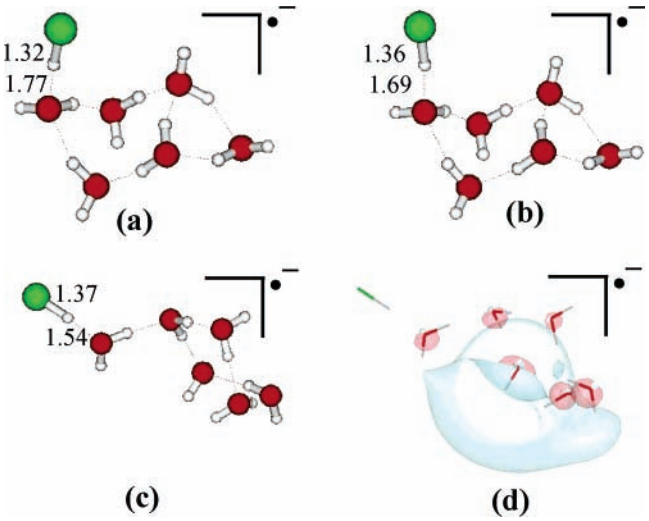

Figure 7. Structures observed for (HCl(1)/6) with HCl on O5. (a) the initial neutral. (b) the anion optimized with the $(H_2O)_6$ base frozen and (c) with no restrictions. (d) contour for the DBS SOMO of structure (c) containing 0.5 electron; Cl··H and H··O distance are given in Å.

tion of the (HCl(3)/12) case, where there is no separation in the upper layer.

4. Singly Coordinated HCl$(H_2O)_6$ Systems: (HCl(1)/6). Studies were made with HCl H-bonded to oxygens 2, 3, 4, and 5 of the amorphous $(H_2O)_6$ (Figure 2(b)). For these four systems, VBEs were obtained from CCSD(T) calculations, as well as B3LYP/aug-cc-pVDZ calculations, on the B3LYP/6-31+G(d) geometries of the neutrals. The CCSD(T) calculations were carried out with 6-31+G(d) basis sets on O atoms and 6-31G-(d) on Cl and H, and 4sp functions added on atoms near the positive ends of the dipoles of the neutrals. The observed HCl VBEs, dipole moments and Cl···H···O bond parameters of the (HCl(1)/6) species are presented in Table 1. These parameters are explained by reference to the system with HCl H-bonded to O5, for which Figure 7, parts a−c, respectively, show structures of the neutral and of the anion at two stages of optimization.

The neutral adduct was formed by placing HCl on the desired site and optimizing at B3LYP/6-31+G(d) level with the ice base frozen. This probably overemphasizes the constraining effect of the lower layers in multilayered structures at 20 K. However, it was considered to be preferable to err in this direction. The presence of HCl on O5 causes the dipole moment to rise from 0.58 D to 2.45 (Table 1). The VBE at the CCSD(T) level is very small, but positive: 0.00063 eV. As is generally found, the B3LYP result is larger: 0.094 eV. The first optimization of the anion is at the B3LYP/6-31+G(d) level and also with the ice base frozen. It led to minor changes in bond angles (Figure 7b), and a movement of the H-bonding H from Cl toward O (compare $r_{(H-Cl)}$ in columns 6 and 7, and $r_{(O\cdots H)}$ in 8 and 9 of Table 1). Notably there is no tendency for the Cl coordination to increase. In fact the Cl moves away from the dangling Hs. A minor increase in electron binding at the B3LYP level from 0.09 to 0.12 eV (not shown in the Table) also occurred. The results in Table 1 for binding to the other Os on the amorphous systems were obtained in the same way and in general exhibit similar increases in dipole moment on HCl binding, positive VBE and changes in Cl···H···O geometry on first constrained optimization.

Studies were also made with HCl H-bonded on O4 and O5 of the hexagonal ice structure of Figure 2c. In these cases, the dipole moment of the initial ice, 4.4 D, is already large, but, as shown in Table 1, it increases further with HCl addition. The B3LYP calculated VBEs are therefore larger than for the systems on amorphous ice and in fact so large that confirmation of DBS formation does not require CCSD(T) calculations. However, the geometry changes on the first optimizations of the anions are similar to those described above. The high dipole moment of hexagonal ice probably also contributes to the larger HCl binding energies shown in column 3 for those systems: the HCl is bonded to the backside of the structure in Figure 2c and aligns with the dipoles caused by the dangling Hs. Only the upper and lower limits of the BEs of the amorphous $(H_2O)_6$ systems have been plotted in Figure 3.

The nature of the electron binding was probed further by carrying out completely unrestricted B3LYP/aug-cc-pVDZ level optimizations for the amorphous systems with HCl on O4 and O5 and the hexagonal system with HCl on O5. In all cases, the Cl moved further away from the plane of the $(H_2O)_6$ and the structure became more elongated. Also within the Cl···H···O bond, the movement of H toward O continues. In the optimized geometry for the O5 amorphous case shown in Figure 7c, the Cl···H is 1.37 Å and H···O decreases to 1.54 Å. Another feature common to these systems was the formation of a five membered ring with the HCl bonded to it via the ejected water. These changes all assisted in the enhancement of the dipole moment. For the O5 amorphous case, the EBE at B3LYP level increased by 0.52 V to 0.61 eV, and the SOMO electron distribution, which is centered around the water protons, became tighter

TABLE 1: $(H_2O)_6$ Cluster HCl Binding Energy on the Born Oppenheimer Surface, Dipole Moment, VBE (Vertical Electron Binding Energies), and Bond Lengths for Neutrals, and Bond Lengths for Anions after Constrained Optimization[a]

					H−Cl (Å)		O···H (Å)	
ice form:	H acceptor	B−O binding energy/kJ mol^{-1}	neutral dipole/D	VBE/eV	neutral	anion	neutral	anion
amorphous	no HCl		0.58	negative				
	O2	23	2.82	0.16 (0.008)	1.31	1.36	1.83	1.72
	O3	25	2.94	0.15 (0.0008)	1.32	1.36	1.81	1.67
	O4	32	2.95	0.16 (0.0012)	1.33	1.38	1.74	1.57
	O5	30	2.45	0.094 (0.0006)	1.32	1.36	1.77	1.69
hexagonal	no HCl		4.4	0.22				
	O4	65	6.14	0.36	1.36	1.51	1.63	1.30
	O5	41	6.25	0.38	1.32	1.35	1.82	1.74

[a] VBEs in parenthesis are from CCSD(T) single-point energies, all other data from B3LYP calculations.

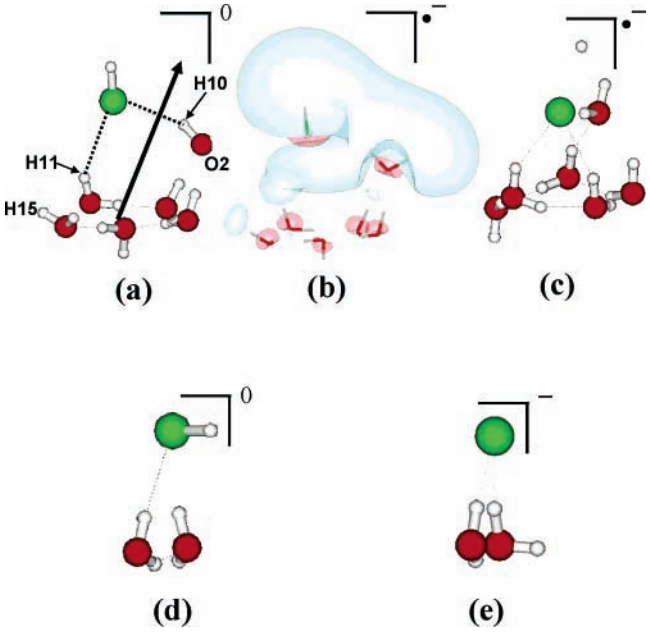

Figure 8. Structures observed for HO−H···ClH coordination. (a) the optimized $HCl(H_2O)_6$ neutral. (b) contour for the DBS′ SOMO on the geometry of (a) containing 0.5 electron. (c) the optimized $H^\bullet$ + $Cl^-(H_2O)_6$ cluster from dissociation. (d) the $HCl(H_2O)_2$ model used to investigate the energy profile for DEA in Figure 9. (e) the $Cl^-(H_2O)_2$ product.

(Figure 7d). Similar behavior was observed for the O4 amorphous system and the O5 hexagonal system. Thus, for these (HCl(1)/6) singly coordinated complexes, the preferred means of stabilization is through elongation and a consequent increase of dipole moment, rather than an increase in coordination to Cl.

In summary, single coordination binding of HCl to all of the sites examined gave rise to dipole moments above the critical value for DBS formation. All had small positive VBEs and stabilization occurred by structural changes that increased the dipole moments.

5. HO−H···Cl−H Coordination. This coordination model was developed by allowing the HCl dipole to interact with the dipoles of the dangling Hs H10 and H11 of the hexagonal $(H_2O)_6$ cluster (Figure 2c). It is worth realizing here that the alternative of aligning the HCl proton to H-bond to O6 and allowing H10 and H11 to form secondary H-bonds (analogous to the (HCl(3)/12) model in Figure 1b1 of section 2) would give more favorable binding. However, the ability of the dipole interactions to prevent formation of the Cl−H···O bond was tested. The neutral structure was optimized at the B3LYP/6-31+g(d) level with no geometric restrictions. One water (the O2 water) was ejected from the ring, giving the geometry shown in Figure 8a, which has one weak HO−H···Cl bond: H10···Cl (r = 2.678 Å), and a minor interaction: H11···Cl (r = 3.419 Å). The HCl BE in this optimized structure relative to the amorphous $(H_2O)_6$ was 14 kJ mol^{-1}, and this is plotted in Figure 3.[36] Continuation of the optimization with analytical force constants indicated that this structure corresponded to a plateau on the BOs. After many steps the H of the HCl moiety rotated to form a 2 coordinated cyclic array of three Os and the ClH with a Cl−H··O bond. The final structure was 39 kJ mol^{-1} lower in energy.

The neutral in Figure 8a has a dipole moment of 7.82 D and formed a temporary DBS with VBE of 0.26 eV at the B3LYP/aug-cc-pVDZ level. The SOMO of this is shown in Figure 8b. Optimization of the anion led to the structure in Figure 8c, for

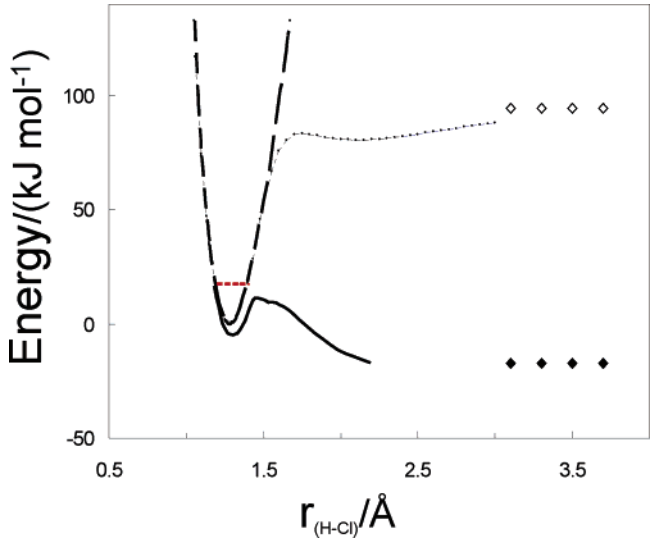

Figure 9. Energy profile for DEA of $HCl(H_2O)_2$ with only HO−H···ClH coordination. Heavy solid line: MP2 computed energy profile for $HCl(H_2O)_2$ anion; heavy dashed lines: PE curve and ZPE of neutral HCl; light dashed line energy profile for HCl dissociation, from ref 38; open and solid diamonds asymptotic levels of the dissociation products for HCl and the clustered system, respectively.

which the energy is 96 kJ mol^{-1} lower. The Cl−H bond has dissociated, and the solvation of the Cl^- has increased by formation of a third HO−H···Cl bond involving H15. The energy profile for dissociative electron attachment (DEA) for this type of HCl binding was modeled with the smaller $HCl(H_2O)_2$ anion structure in Figure 8d. The energy was examined as a function of $r_{(H-Cl)}$ with all other parameters optimized.[37] The heavy solid line in Figure 9 shows the energy profile of the anion system computed at the MP2 level. The potential energy curve and ZPE of neutral HCl, which would not be distorted significantly by the hydrogen bonds to Cl,[38,39] is given by the heavy dashed lines for comparison (data from ref 38). For both HCl and $HCl(H_2O)_2$, the reference energy is the energy of the neutral at the equilibrium $r_{(H-Cl)}$. The open and solid diamonds show the asymptotic levels of the dissociation products for HCl and the clustered system, respectively. The calculation indicates that the barrier to dissociation now lies below the ZPE for the H−Cl vibration and the structure therefore dissociates to $H^\bullet$ and solvated $Cl^-(H_2O)_2$, the optimized geometry of which is shown in Figure 8e. In effect, it is evident that coordination of HCl by these seemingly weak HO−H···Cl interactions will in general lead to spontaneous dissociation.

Discussion

Comparisons of Different Coordination Systems. Representative models of HCl bound to H_2O clusters in singly, doubly, and triply coordinating sites have been prepared to simulate HCl attachment at sites in amorphous ice. Five singly coordinated Cl−H···O sites on $(H_2O)_6$ clusters were studied (Table 1 and Figure 7), and a $(H_2O)_6$ cluster was also used to investigate HO−H···Cl−H interactions (Figure 8). One doubly coordinated (HCl(2)/n) structures of n = 12 (Figure 5) was employed, exploring the effect of having a bilayer. A bilayer $(H_2O)_{12}$ cluster was also employed for the triply coordinated model. As found in earlier studies of neutral $HCl(H_2O)_n$ clusters,[4,6,7] the polarization of the Cl−H bond in primary Cl−H···O hydrogen bonds increases and the H moves closer to the O atom with increasing coordination. However, the only system that could be considered to be fully ionized to a $Cl^-\cdots HOH_2^+$ ion pair in this work was

the triply coordinated (HCl(3)/12) in Figure 4d, which underwent the electron induced rearrangement. As seen in Figure 3, the smallest HCl BE was for the HO−H···Cl−H interaction. The BEs for Cl−H··O single coordination sites varied from 23 to 32 kJ mol^{-1}, and as expected, successive addition of HO−H···Cl−H bonds to this primary interaction caused further sequential increases. The two (HCl(3)/12) neutrals have BEs of 55 and 76 kJ mol^{-1}, the latter being for the rearranged species containing the $Cl^-\cdots HOH_2^+$ ion pair.

The dipole moments of the neutral HCl adducts were in general larger than the minimum value for dipole binding of an electron, and formation of an initial DBS on the neutral geometry, a DBS′, was the primary step in electron attachment in all cases. For the amorphous $(H_2O)_6$ clusters with low dipole moments, this was confirmed by calculations at the CCSD(T) level. The relaxation processes of the DBS′ from the neutral geometries depended on the number of H_2O and the type of HCl coordination. HO−H···Cl−H interaction totally erodes the potential energy well for the Cl−H vibration and the DBS′ of that structure dissociates spontaneously, Figure 9. The DBS′ of the Cl−H···OH_2 coordinated systems on $(H_2O)_6$ clusters gained stability by becoming more linear and/or planar, which enhances their dipole moments, increases the electron binding and thus lowers the energy. The initial optimizations with the $(H_2O)_6$ cluster frozen caused the polarization of the Cl−H···OH_2 bond to increase beyond that of the neutral with the H moving still closer to O (Table 1, columns 6−9), which is an important contributor to the increase in dipole moment. None of three $(H_2O)_6$ clusters for which unrestricted optimization was carried out (e.g., Figure 7c) showed any signs of increasing the coordination to Cl.

The relaxation processes for the larger (HCl(2)/12) and (HCl-(3)/12) systems were more interesting and complex. The pathways seen here are not necessarily unique, but for both $x = 2$ and 3 the first step was the formation of a $Cl^-\cdots HOH_2^+$ ion pair, the presence of which strongly increased the dipole moment and EBE of the network. Rearrangement of the protons then occurred, and the Cl^- eventually became solvated by three HO−H···Cl^- bonds, causing a further increase in stability. The electron-induced proton rearrangements resemble those reported in other systems,[40] and the enhancement of the dipole binding field by the ion pair formation seen here is similar to the findings in ref 18. Quite remarkable is the tightly bound electron structure in Figure 5b1,2,3, where the SOMO is shrunk almost to the dimensions of a solvated electron. With the $HCl(H_2O)_{12}$ systems, reaction of the excess electron with H_3O^+ to form H• atoms is very favorable. However, we also find that rearrangement may lead to very stable DBS structures (Results: section 3 and Figures 4b and 5b), and these may be long-lived. Indeed, the inherent stability of the DBS structures is emphasized for all types of HCl coordination except HO−H···Cl−H.

Implications for the Amorphous H_2O Ice Film Experiments at 20 K. Electrons injected into pure ice may initially be localized as DBS and subsequently move to deeper traps, which may in part preexist as defects and/or be formed by solvent relaxation.[41,42] Our hexagonal ice models (Figure 1, parts a1 and a2) contained dangling Hs which caused dipole moments to be well in excess of the critical value for electron binding. However, as pointed out in the Results section 1.b, the number of sites of high dipole moment in an amorphous structure will not be as large, since the tendency to minimize the surface energy will reduce the number of dangling Hs. The experiments of ref 10 showed that the presence of 0.2 monolayers (ML) of HCl on a 5 ML H_2O ice film increased the electron trapping coefficient from 80, the value observed on ice alone,[43] to 250 mV s^{-1} nA^{-1}. The 0.2 ML of HCl in effect more than triples the number of traps. On a per molecule basis this requires the electron capture cross section for HCl to be 4×10^{-15} cm^2 at 0.0 eV.[10] In the Results: section 5 we have seen that HO−H···Cl−H coordination totally changes the PE surface for DEA by HCl and brings the threshold to zero energy (Figure 9). Under such circumstances, the DEA cross section would approach the theoretical maximum ($\sim 2 \times 10^{-14}$ cm^{-2} [44]), and if 13% of the HCl were bound this way, the increased trapping coefficient could be explained. However, HO−H···Cl−H coordination is not likely to be common, and this process alone cannot account for the effect. In the first place, HO−H···Cl−H is the weakest interaction (Figure 3). Second sites with suitable dangling Hs for this type of binding are likely to be less common than those for Cl−H···O binding. Thus, the majority of HCl molecules added to the preformed 5 ML H_2O ice film should undergo Cl−H···O single coordination with a few forming secondary HO−H···Cl bonds. The present ab initio results show that the neutrals of all of these systems can form DBS. Thus, this mode of trapping would appear to be the major means by which HCl enhances the trapping coefficient. Another key point is that Cl−H···O single coordination to the $(H_2O)_6$ amorphous ice model caused the dipole moment to rise from 0.58 D to above 2.4 D for all of the sites investigated (Table 1). Thus, HCl addition could clearly enhance the number of sites with dipole moment above the threshold for DBS formation.

Implications for Polar Stratospheric Clouds. The temperature in polar stratospheric clouds is near 190 K,[8,9] much higher than in the experiments of ref 10. Thus, the H_2O mobility in surface layers is increased. Under these circumstances, H_2O motion would enhance chloride solvation, converting (HCl(1)/*n*) and (HCl(2)/*n*) forms to triply coordinated (HCl(3)/*n*) species. Indeed there are indications that HCl in neutral ice at this temperature is fully ionized.[45] Thus, the strong dipoles due to $Cl^-\cdots H-OH_2^+$ would already exist, and electron trapping would be enhanced. The higher mobility would facilitate relaxation to deeper traps. Reaction 1 would therefore become extremely important.[46,47] This leads to production of a hydrogen atom, which has the potential to escape from the ice particle.

Lu and Sanche pointed out in ref 10 that ice particles would be ionized by cosmic rays at a rate 4 orders of magnitude greater than air ionization and suggested that this might contribute to the production of species that cause ozone depletion.[48] The correlations of Cosmic ray intensity with ozone loss, to which they drew attention, have been disputed.[49−51] However, we believe it is important to point out the following facts. The process of cosmic ray ionization in ice leads to hole formation, i.e., $H_3O^+ + OH^•$, as well as electron production. In the absence of electron traps, like HCl, a high proportion of holes and electrons recombine.[42] Trapping of the electron will inhibit this recombination. Escape of either the OH• hole product or the H• is potentially harmful, since both participate in catalytic reactions which remove ozone,[52] viz

$$H^• + O_2 + M \rightarrow HO_2^• \quad (2)$$

$$HO_2^• + O_3 \rightarrow OH^• + 2O_2 \quad (3)$$

$$OH^• + O_3 \rightarrow HO_2^• + O_2 \quad (4)$$

It is important to note that any electron trap in the ice particles will have a similar effect. In this regard HNO_3 and H_2SO_4 are likely to behave in a manner similar to HCl. The chlorine

reservoir molecule $ClONO_2$ is also a candidate for this, since it might have a high rate of DEA in reaction 5, viz

$$e^- + ClONO_2 \rightarrow Cl^\bullet + NO_3^- \quad (5)$$

During winter in the absence of sunlight at the poles, these cosmic ray derived processes provide an alternative route to the ice surface heterogeneous reactions in PSCs, viz

$$HCl + ClONO_2 \rightarrow Cl_2 + HNO_3 \quad (6)$$

In the spring, reaction 7, which produces the damaging $Cl^\bullet$ atoms,[52] becomes possible

$$Cl_2 + h\upsilon \rightarrow 2Cl^\bullet \quad (7)$$

whereas reactions 2, 3, and 4 are always effective. The relative contribution from cosmic radiation will depend on the rate of ionization relative to that of reactions 6 + 7. The situation is complicated by another factor which is the size of the ice particles. Since these are small, an electron created by ionization will likely escape from the primary ice particle, leaving the $OH^\bullet$ of the hole free. The electron may re-enter a second ice particle to react as outlined above, but more likely will be captured by oxygen to form $O_2^{\bullet -}$. It is not clear how well these processes are taken into account in current atmospheric models.

Acknowledgment. The financial support of the Natural Sciences and Engineering Research Council of Canada, the Canadians Institutes of Health Research and the University of Calgary is gratefully acknowledged. The authors are also indebted to Mr. Patrick Brunelle for assistance with the computer network and to one of the reviewers who drew our attention to ref 16.

Supporting Information Available: Tables containing supplimentary material. This material is available free of charge via the Internet at http://pubs.acs.org.

References and Notes

(1) Bolton, K.; Pettersson, J. B. C. *J. Am. Chem. Soc*. **2001**, *123*, 7360.
(2) Svanberg, M.; Pettersson, J. B. C.; Bolton, K. *J. Phys. Chem. A* **2000**, *104*, 5787.
(3) Sadtchenko, V.; Giese, C. F.; Gentry, W. R. *J. Phys. Chem. B* **2000**, *104*, 9421−9429.
(4) Milet, M.; Struniewicz, C.; Moszynski, R.; Wormer, P. *J. Chem. Phys.* **2001**, *115*, 349.
(5) Buch, V.; Sadlej, J.; Aytemiz-Uras, N.; Devlin, J. P. *J. Phys. Chem. A* **2002**, *106*, 9374−9389.
(6) Devlin, J. P.; Uras, N.; Sadlej, J.; Buch, V. *Nature* **2002**, *417*, 269−271.
(7) Huneycut, A. J.; Saykally, R. J. *Science* **2003**, *299*, 1329.
(8) Solomon, S. *Rev. Geophys*. **1988**, *26*, 131.
(9) Tuomi, R.; Jones, R. L.; Pyle, J. A. *Nature* **1993**, *365*, 37.
(10) Lu, Q.-B.; Sanche, L. *J. Chem. Phys*. **2001**, *115*, 5711.
(11) Abbatt, J. P. D. *Chem. Rev.* **2003**, *103*, 4783.
(12) Azria, R.; Coat, Y. Le.; Lachgar, M.; Tronc, M.; Parenteau, L.; Sanche, L. *Surf. Sci.* **2000**, *451*, 91.
(13) Chipman, D. M. *J. Phys. Chem.* **1979**, *83*, 1657.
(14) Skurski, P.; Gutowski, M. *J. Chem. Phys*. **1999**, *111*, 3004.
(15) Hendricks, J. H.; de Clercq, H. L.; Lyapustina, S. A.; Bowen, K. H. *J. Chem. Phys.* **1997**, *107*, 2962.
(16) Ayotte, P.; Weddie, G. H.; Bailey, C. G.; Johnson, M. A.; Vila, F.; Jordan, K. D. *J. Chem. Phys*. **1999**, *110*, 6268.
(17) Lee, H. M.; Kim, K. S. *J. Chem. Phys.* **2002**, *117*, 706.
(18) Sobolewski, A. J.; Domcke, W. *Phys. Chem. Chem. Phys.* **2002**, *4*, 4.
(19) Sobolewski, A. L.; Domcke, W. *Phys. Chem. Chem. Phys.* **2003**, *5*, 1130.
(20) Frisch, M. J.; Trucks, G. W.; Schlegel, H. B.; Scuseria, G. E.; Robb, M. A.; Cheeseman, J. R.; Zakrzewski, V. G.; Montgomery, J. A., Jr.; Stratmann, R. E.; Burant, J. C.; Dapprich, S.; Millam, J. M.; Daniels, A. D.; Kudin, K. N.; Strain, M. C.; Farkas, O.; Tomasi, J.; Barone, V.; Cossi, M.; Cammi, R.; Mennucci, B.; Pomelli, C.; Adamo, C.; Clifford, S.; Ochterski, J.; Petersson, G. A.; Ayala, P. Y.; Cui, Q.; Morokuma, K.; Malick, D. K.; Rabuck, A. D.; Raghavachari, K.; Foresman, J. B.; Cioslowski, J.; Ortiz, J. V.; Stefanov, B. B.; Liu, G.; Liashenko, A.; Piskorz, P.; Komaromi, I.; Gomperts, R.; Martin, R. L.; Fox, D. J.; Keith, T.; Al-Laham, M. A.; Peng, C. Y.; Nanayakkara, A.; Gonzalez, C.; Challacombe, M.; Gill, P. M. W.; Johnson, B. G.; Chen, W.; Wong, M. W.; Andres, J. L.; Head-Gordon, M.; Replogle, E. S.; Pople, J. A. *Gaussian 98*, revision A.7; Gaussian, Inc.: Pittsburgh, PA, 1998.
(21) Frisch, M. J.; Trucks, G. W.; Schlegel, H. B.; Scuseria, G. E.; Robb, M. A.; Cheeseman, J. R.; Montgomery, Jr., J. A.; Vreven, T.; Kudin, K. N.; Burant, J. C.; Millam, J. M.; Iyengar, S. S.; Tomasi, J.; Barone, V.; Mennucci, B.; Cossi, M.; Scalmani, G.; Rega, N.; Petersson, G. A.; Nakatsuji, H.; Hada, M.; Ehara, M.; Toyota, K.; Fukuda, R.; Hasegawa, J.; Ishida, M.; Nakajima, T.; Honda, Y.; Kitao, O.; Nakai, H.; Klene, M.; Li, X.; Knox, J. E.; Hratchian, H. P.; Cross, J. B.; Bakken, V.; Adamo, C.; Jaramillo, J.; Gomperts, R.; Stratmann, R. E.; Yazyev, O.; Austin, A. J.; Cammi, R.; Pomelli, C.; Ochterski, J. W.; Ayala, P. Y.; Morokuma, K.; Voth, G. A.; Salvador, P.; Dannenberg, J. J.; Zakrzewski, V. G.; Dapprich, S.; Daniels, A. D.; Strain, M. C.; Farkas, O.; Malick, D. K.; Rabuck, A. D.; Raghavachari, K.; Foresman, J. B.; Ortiz, J. V.; Cui, Q.; Baboul, A. G.; Clifford, S.; Cioslowski, J.; Stefanov, B. B.; Liu, G.; Liashenko, A.; Piskorz, P.; Komaromi, I.; Martin, R. L.; Fox, D. J.; Keith, T.; Al-Laham, M. A.; Peng, C. Y.; Nanayakkara, A.; Challacombe, M.; Gill, P. M. W.; Johnson, B.; Chen, W.; Wong, M. W.; Gonzalez, C.; Pople, J. A. *Gaussian 03*, Revision B.05; Gaussian, Inc., Wallingford CT, 2004.
(22) Kobko, N.; Dannenberg, J. J. *J. Phys. Chem. A* **2001**, *105*, 1944.
(23) The ability of the B3LYP procedure to handle $Cl^-\cdot nH_2O$ clusters was checked by calculating the energies of the reaction: $nH_2O + HCl + e^- \rightarrow H^\bullet + Cl^-\cdot nH_2O$ using aug-cc-pVDZ basis sets on H and O and 6-311+G(3df,2p) on Cl. The results were −36.1 and −80.7 kJ mol^{-1} for $n = 2$ and 3, respectively. These compare exceedingly well with −28.3 and −77.3 kJ mol^{-1} derived from experimental data in Wagman, D. D.; Evans, W. H.; Parker, V. B.; Schumm, R. H.; Halow, I.; Bailey, S. M.; Churney, K. L.; Nuttal, R. L. *J. Chem. Phys. Ref. Data* **1982**, *11*, Suppl. No. 2 and Kebarle, P. *Annu. Rev. Phys. Chem.* **1977**, *28*, 445.
(24) Rak, J.; Skurski, P.; Gutowski, M. *J. Chem. Phys*. **2001**, *114*, 10673.
(25) Gutowski, M.; Hall, C. S.; Adamowicz, L.; Hendrics, J. H.; de Clercq, H. L.; Lyapustina, S. A.; Nilles, J. M.; Xu, S.-J.; Bowen, K. H., Jr. *Phys. Rev. Lett.* **2002**, *88*, 143001−1.
(26) This relation between DBS and neutral frequencies is also exhibited by the smaller (HCl(2)/2) and (HCl(2)/3) analogues of the systems studied here. Rauk, A.; Armstrong, D. A. To be published.
(27) gOpenMol, http://www.csc.fi/gopenmol/.
(28) Losada, M.; Leutwyler, S. *J. Chem. Phys.* **2002**, *117*, 2003.
(29) Casassa, S.; Ungliengo, P.; Pisani, C. *J. Chem. Phys*. **1997**, *106*, 8030.
(30) Longsdale, K. *Proc. R. Soc*. **1958**, *A247*, 424.
(31) Materer, N.; Starke, U.; Barbieri, A.; Van Hove, M.; Somorjai, A. G. A.; Kroes, G.-J.; Minot, C. *J. Phys. Chem.* **1995**, *99*, 6267.
(32) Desfrançois, C.; Abdoul-Carime, H.; Khelifa, N.; Scherman, J. P. *Phys. Rev. Lett*. **1994**, *73*, 2436 and references therein.
(33) Sarasola, C.; Fowler, J. E.; Ugalde, J. M. *J. Chem. Phys.* **1999**, *110*, 11717.
(34) As an indication of what the error due to over binding by the B3LYP procedure in the converged 0.553 eV value might be, one may compare the case of the $(H_2O)_6$ chain cluster of ref 16. Here a B3LYP EBE, converged with three sets of diffuse functions and a 6-31+G(2d,p) basis set, was used to calculate a vertical detachment energy. The B3LYP value was 0.64 eV as compared to the experimental value of 0.45 eV, an error of ∼0.2 eV.
(35) Lee, H. M.; Kim, K. S. *J. Chem. Phys.* **2002**, *117*, 706.
(36) The HCl BE for the interaction with the hexagonal $(H_2O)_6$ structure before optimization was very similar: 16 kJ mol^{-1}.
(37) The neutral form of this is not an optimized structure because the lowest $HCl(H_2O)_2$ structure is cyclic: Buch, V.; Sadlej, J.; Aytemiz-Uras, N.; Devlin, J. P. *J. Phys, Chem. A* **2002**, *106*, 9374−9389.
(38) Rauk, A.; Armstrong, D. A. *Int. J. Quantum Chem*. **2003**, *95*, 683; **2004**, *96*, 69.
(39) Rauk, A.; Armstrong, D. A. *J. Phys. Chem. A* **2000**, *104*, 7651.
(40) Haranczyk, M.; Bachorz, R.; Rak, J.; Gutowski, M.; Radisic, D.; Stokes, S. T.; Nilles, J. M.; Bowen, K. H. *J. Phys. Chem B* **2003**, B *107*, 7889.
(41) Pommeret, S.; Gauduel, Y. *J. Phys. Chem.* **1991**, *95*, 4126.
(42) Gillis, H. A.; Quickenden, T. I. *Can. J. Chem.* **2001**, *79*, 80.
(43) Lu, Q. B.; Sanche, L. *Phys. Rev. B* **2002**, 63, 153403.
(44) Compton, R. N.; Huebner, R. H. *Advances in Radiation Chemistry*; Burton, M., Magee, J. L., Eds.; Wiley: New York, 1970; Vol. 2, p 281.
(45) Kang, H.; Shin, T.-H.; Park, S.-C.; Kim, I. K.; Han, S.-J. *J. Am. Chem. Soc*. **2000**, 122, 9842.

(46) With the HCl largely ionized the electron would in effect react with the H_3O^+ as it does in liquid water: see ref 47.
(47) Buxton, G. V. In *Radiation Chemistry: Principles and Applicaions*; Fahartaziz, Rodgers, M. A. J., Eds.; VCH: New York, 1987; Chapter 10.
(48) Lu, Q.-B.; Sanche, L.; *Phys. Rev. Lett*. **2001**, *87*, 078501−1.
(49) Harris, N. R. P.; Farman, J. C.; Fahey, D. W. *Phys. Rev. Lett*. **2002**, *89*, 219801−1.
(50) Patra, P. K.; Santhanan, M. S. *Phys. Rev. Lett*. **2002**, *89*, 219803−1.
(51) Müller, R. *Phys. Rev. Lett*. **2003**, *91*, 058502−1.
(52) Solomon, S. *Rev. Geophys.* **1999**, *37*, 275.